HHS Public Access

Author manuscript

Mol Cancer Res. Author manuscript; available in PMC 2022 August 07.

Published in final edited form as:

Mol Cancer Res. 2022 August 05; 20(8): 1284–1294. doi:10.1158/1541-7786.MCR-21-0905.

Caspase-9b drives cellular transformation, lung inflammation, and lung tumorigenesis

Minjung Kim[1,*], **Ngoc T. Vu**[1], **Xue Wang**[1], **Gamze B. Bulut**[2], **Min-Hsuan Wang**[3], **Cora Uram-Tuculescu**[4], **Raghavendra Pillappa**[4], **Sungjune Kim**[3], **Charles E. Chalfant**[1,5,6,7,*,#]

[1]Department of Cell Biology, Microbiology, and Molecular Biology, University of South Florida, Tampa, FL 33620

[2]Department of Biochemistry and Molecular Biology, Virginia Commonwealth University, Richmond VA, 23298

[3]Departments of Immunology and Radiology, The Moffitt Cancer Center, Tampa, FL 33612

[4]Department of Pathology, Virginia Commonwealth University (VCU), Richmond, Virginia 23298, USA

[5]Departments of Cell Biology and Medicine, Division of Hematology & Oncology, University of Virginia, Charlottesville, VA, 22903

[6]Program in Cancer Biology, University of Virginia Cancer Center, Charlottesville, VA, 22903

[7]Research Service, Richmond Veterans Administration Medical Center, Richmond VA, 23298

Abstract

Caspase 9 undergoes alternative splicing to produce two opposing isoforms: pro-apoptotic Caspase-9a (C9a) and pro-survival Caspase-9b (C9b). Previously, our laboratory reported that C9b is expressed in majority of non-small cell lung cancer tumors and directly activates the NF-κB pathway. In this study, the role of C9b in activation of the NF-κB pathway *in vivo*, lung inflammation and immune responses, and lung tumorigenesis were examined. Specifically, a transgenic mouse model expressing human C9b in the lung pneumocytes developed inflammatory lung lesions, which correlated with enhanced activation of the NF-κB pathway and increased influx of immunosuppressive MDSCs in contrast to wild-type mice. C9b mice presented with facial dermatitis, a thickened and disorganized dermis, enhanced collagen depth, and increased serum levels of IL-6. C9b mice also developed spontaneous lung tumors, and C9b cooperated with oncogenic *KRAS* in lung tumorigenesis. C9b expression also cooperated with oncogenic *KRAS* and p53 downregulation to drive the full cell transformation of human bronchial epithelial cells (e.g., tumor formation).

[#]To whom correspondence should be addressed: Charles E. Chalfant, Professor, Department of Medicine, Division of Hematology & Oncology, P.O. Box 801398, University of Virginia, Charlottesville, VA, 22903, cechalfant@virginia.edu or charles.chalfant@va.gov.
[*]Contributed equally to the presented study.

The authors have declared that no conflict of interest exists.

Implications: Our findings show that C9b can directly activate NF-κB pathway *in vivo* to modulate lung inflammation, immune cell influx, and peripheral immune responses, which demonstrates that C9b is key factor in driving cell transformation and lung tumorigenesis.

Keywords

Caspase-9b; inflammation; NF-κB pathway; caspase 9; RNA splicing; tumorigenesis; oncogenes; cell transformation; lung cancer; lung

INTRODUCTION

Caspase 9 is a member of the caspase family and an important mediator of intrinsic apoptosis via association with cytochrome C and Apaf-1 to form the apoptosome (1,2). The *CAS9* gene is also controversially reported as a tumor suppressor (3). Pre-mRNA produced from the *CAS9* gene can be alternatively spliced by inclusion or exclusion of the four-exon cassette (exons 3,4,5,6) to produce two isoforms: pro-apoptotic caspase 9a (C9a) and anti-apoptotic caspase 9b (C9b) (4,5). C9b mRNA lacks the exon 3,4,5,6 cassette, which encodes the large subunit and the catalytic domain, but the translated protein retains the APAF-1 and cIAP-1 association regions. C9b competes with C9a in binding to the apoptosome complex, inhibits the activation of C9a and the ability of a number of cell death agonists to induce apoptosis and the loss of cell viability (4,5). Therefore, the alternative splicing of caspase 9 pre-mRNA is a key step in determining the apoptotic fate of a cell (2).

In studies focused on the cellular mechanisms regulated by C9b, ablation of C9a did not produce the same biological phenotypes of enhanced cell survival, anchorage-independent growth (AIG), and tumorigenesis observed for C9b expression (6-8). These findings showed that C9b had a “gain of function” in addition to competing with C9a for the APAF-1 association. C9b was shown to activate the canonical nuclear factor-kappaB pathway (NF-κB) pathway via direct interaction with the cellular inhibitor of apoptosis 1 (cIAP1) (6).

The NF-κB pathway is the master regulator of inflammation and is tightly linked to cancer as a pro-survival and oncogenic pathway (9) . Suppression of NF-κB in myeloid cells or tumor cells induces tumor regression (10). In relation to NSCLC, both the Baldwin and Jacks laboratories demonstrated that the NF-κB pathway cooperates with oncogenic *RAS* to enhance tumorigenesis in mice (11,12). Induction of airway epithelial NF-κB during allergic inflammation was shown to cause airway hyperresponsiveness by increasing lymphocytes and neutrophils in the bronchioalveolar lavage (BAL) fluid (13,14). Moreover, sustained NF-κB signaling induced chronic inflammation and emphysema by four months of age. By eleven months, NF-κB activated mice develop lung adenomas, which recruit M2-polarized macrophages and regulatory T lymphocytes providing a pro-tumorigenic microenvironment (15).

Due to our finding that C9b induced activation of the NF-κB pathway and high C9b expression occurs in >78% of non-small cell lung cancers (NSCLCs) (6-8), our laboratory developed a C9b transgenic mouse model and found that C9b expression in lung pneumocytes was sufficient to activate the NF-κB pathway and induce the infiltration of lymphocytes in the lungs linked to increased IL-6 levels and facial dermatitis. Furthermore,

C9b expression induced lung adenocarcinoma formation in aged mice and cooperated with oncogenic *KRAS* to induce lung tumorigenesis demonstrating a major pro-tumor function for this caspase 9 splice variant.

MATERIALS AND METHODS

Detailed materials and methods and the list of key reagents and resources (Supplementary table 1) can be found in Supplementary Information.

Cell culture and *in vitro* assays:

HBEC-3KT (Obtained from ATCC) and HBEC3KT-KP cells with $KRAS^{G12V}$ expressing (/K) ± p53 shRNA downregulated (/P) (a gift from Drs. John Minna and Jerry Shay (16)) were cultured as described (10). HBEC3KT-KP cells were authenticated via western immunoblotting and qPCR for p53 and $KRAS^{G12V}$. MLE12 cells (Obtained from ATCC) were cultured as described (17). These cell lines were transduced with pLEX304-eGFP, -WT C9b, or -AT/GG Mut C9b lentivirus treated with 8 μg/mL polybrene (Sigma) and selected with blasticidin. MLE12/K and HBEC-3KT/K cells are generated by transducing cells with pLenti6-$KRAS^{G12V}$ (addgene). Plate colony formation assays (cell survival) and soft agar colony formation assays (AIG) were undertaken as described (7). All cell lines were used within 6 passages from receipt and thawing. Cell lines were tested every two months for mycoplasma (universal mycoplasma detection kit, ATCC) throughout the study starting two months after thawing cells received from ATCC and immediately for other cell lines herein described. Parental cell lines were authenticated by STR (short tandem repeat) profiling.

Western immunoblotting and immunoprecipitation:

Western immunoblotting was accomplished as described (6) using the following primary antibodies: anti-caspase-9 (Enzo Life Sciences); anti-FLAG (Sigma); RIP1, anti-IκBα, anti-Myc tag, c-Myc, anti-HSP90, and anti-β-actin (Cell Signaling Technology); anti-K-63 Ub (Abcam). Secondary antibodies were horseradish peroxidase-conjugated anti-rabbit IgG and anti-mouse IgG antibodies (Cell Signaling Technology). RIP1 immunoprecipitation was performed as described (6).

Mouse models:

All mouse studies were conducted under the USF approved IACUC proposals, 8191M and 8230R (Assurance number: A-4100-01) and the James A. Haley VAH approved IACUC protocol, #4433V.

Caspase 9b Transgenic Mouse Model: Lung specific transgenic mouse expressing FLAG-tagged human Caspase-9b was designed and generated by the VCU Transgenic/ Knockout Mouse Shared Resource Core. Specifically, the open reading frame expressing human Caspase-9b was inserted between rabbit beta-globin introns downstream of the human SPC promoter sequence. Genotyping PCR was performed using forward (5`-ATA TCT CCG CTG AAG CCG-3') and reverse (5'- ATC TTC GGA AGC TGG CAG T-3') primer sets.

Lung inflammation of C9b mice was semi-quantitatively graded (Score 0-3 as 0 (none) and 3 (severe)) based on the number and the size of peribronchial/bronchiolar/alveolar lymphoid aggregates and diffuse infiltrates observed on H&E images at 10x magnification blinded to the genotypes as described in (18). The alveolar area was calculated by morphometric analyses of trichrome stained images using ImageJ (NIH).

Cohorts of Line 2 and line 4 C9b mice were compared to littermate transgene negative/control mice for the development of skin dermatitis from 3 months to 23 months of age. Mice with deep ulcerative skin lesions penetrating through both the epidermis and dermis were identified during routine daily health checks blinded to the genotype of the mice as described (19). Mice with a simple alopecia/hair loss or a focal superficial mild skin lesion or with fighting wounds were not counted.

KRAS Lung Tumor Mouse Model: Seven to eight-week-old *KRAS*$^{G12D\ L/+}$ mice (20) were intratracheally instilled with 2.5 x 10^7 purified lentiviral particles. Mice were euthanized at 32 wks post instillation.

Mouse Tumor Xenograft Model: 5-week-old female NOD/SCID (Envigo) mice were injected subcutaneously into hind flanks with 2.5 x10^6 HBEC-3KT/KP cells (mixed in 50% Matrigel solution) expressing GFP (n=10), WT C9b (n=20), or AT/GG Mut C9b (n=10). On day 40 post-implantation, mice with palpable tumors were euthanized, and tumors were excised for histological analyses.

Histology and immunohistochemistry:

Mouse organs (lung, liver, spleen, and skin) and tumors were fixed in 10% formalin and embedded in paraffin for histological and immunohistochemical analyses as described (21,22) utilizing the following primary antibodies: anti-FLAG, -Caspase 9, - IκBα, p65, -pERK, -Myc Tag (Cell Signaling Technology); -SOX2 (Sigma); -Gr1 (Ly6G/6C), IL-6 (Novus Biologicals); -HMGA2 (ThermoFisher, Waltham, MA.); -p63, and -Synaptophysin (Santa Cruz Biotechnology). Gomori Trichrome staining (Richard-Allan Scientific) and Alcian blue-PAS staining (Statlab) were performed following manufacturers' instructions. HMGA2 score was calculated by multiplying staining intensity score (0: no stain, 1: weak, 2: moderate, 3: strong) with % positivity score (0: <5%, 1: <10%, 2: <50%, 3: >50% tumor cells).

Flow cytometry:

Flow cytometric analysis of the immune compartment in murine lung and spleen was performed as described (23). The MDSC subsets within the spleen and lung were characterized by surface staining in PBS containing 5% FBS (FACS buffer) with: Gr1 (BUV395), F4/80 (BV711), CD19 (PerCP-Cy5.5), from BD Biosciences, CD11b (BV605), CD11c (Alexa488), IA/IE (Alexa647), and B220 (APC-H7) from Biolegend, incubated in 4 °C for 1 h, then washed twice with FACS buffer, and finally fixed in PBS containing 1% paraformaldehyde for flow cytometric analysis. Dead cells were excluded using the Zombie Violet Fixable Viability Kit (Biolegend) following the manufacturer's protocol. Cells were

acquired on a BD FACSymphony™ A5 and data were analyzed with FlowJo Version 10.0 software .

Statistical analysis:

Statistical differences between the 2 groups were determined by a 2-tailed, unpaired Student's t-test. Statistical differences among ≥ 3 groups (adjusted *p* values) were determined by ANOVA followed by Tukey's multiple comparison test. All tests were performed using GraphPad Prism 9 software. *P* values of less than 0.05 were considered significant.

RESULTS

C9b activates the NF-κB pathway and cooperates with oncogenic KRAS to induce cellular transformation.

The expression of C9b in NSCLCs enhances tumor phenotypes for NSCLC cells, which required the activation of the NF-κB pathway (6). High C9b expression is also observed in >78% of human NSCLC tumors. The question remained as to whether C9b expression was a consequence of tumorigenesis or an important oncogenic signaling factor in cooperating with oncogenes to facilitate cellular transformation. To study the functional effects of C9b expression toward full malignancy in lung epithelial cells, we utilized the genetically defined CDK4/hTERT-immortalized normal human bronchial epithelial cells (HBEC-3KT) ± common lung cancer oncogenic changes (p53 downregulation via shRNA (P) and ectopic expression of oncogenic *KRAS* (*KRAS*^{G12V}) (K) (Fig. 1A, B). Expression of WT C9b, but not GFP control or the AT/GG Mut C9b (a mutant that retains APAF-1 association and anti-apoptotic capabilities, but cannot bind cIAP-1 and activate the NF-κB pathway (6)), in HBEC-3KT cells increased RIP1 K^{63}-ubiquitination (Fig. 1C) and decreased IκBα (Fig. 1D) demonstrating activation of the NF-κB pathway. The effect on IκBα was blocked by the addition of the IKK inhibitor, BAY11-7082 (Fig. 1D).

Functionally, C9b expression in HBEC-3KT cells increased cell survival/colony formation compared to GFP control and the AT/GG Mut C9b (Fig. 1E), but failed to promote anchorage-independent growth (AIG) (Fig.1F). When *KRAS*^{G12V} is expressed in these cells (HBEC-3KT/K), C9b dramatically and significantly enhanced *in vitro* cellular transformation (e.g., AIG) compared to GFP and AT/GG Mut C9b (Fig. 1G). WT C9b further cooperated with oncogenic *KRAS* to further enhance AIG when there was concomitant p53 downregulation (HBEC-3KT/KP) (Fig. 1G): cell lines which showed insignificant AIG in the GFP control similar to previous reports (Fig. 1G) (16,24). Although significantly lower, AT/GG Mut C9b also increased the AIG capacity of these cell lines compared to GFP control, suggesting a possible role for NF-κB-independent and anti-apoptotic abilities of C9b in cell transformation. C9b expression in HBEC-3KT/KP cells also increased invasion through Matrigel (Fig. 1H). Similar effects were observed in MLE12 mouse lung epithelial cells (SPC+), a cell line derived from a transgenic mouse model with SPC promoter driven SV40 large T antigen (Supplementary Fig. S1) (17). Specifically, C9b expression cooperated with oncogenic *KRAS*, driving AIG and invasion. The enhanced cell survival and induction of *in vitro* cell transformation (e.g., AIG enhancement/induction)

induced by C9b were further shown to require the NF-κB pathway as BAY 11-7082 blocked these phenotypes in MLE12 cells (Supplementary Fig. S1). Enhanced AIG by C9b expression in A549 (lung cancer cell line harboring a $KRAS^{G12C}$ mutation, Supplementary Fig. S2) was suppressed by Bay 11-7082 (Supplementary Fig. S2A,B), which were further reduced by combined treatment with MEK162 (Ras/MEK/ERK pathway inhibitor) (Supplementary Fig. S2B), supporting cooperation of oncogenic *KRAS* and NF-κB pathways. These cells with reduced C9b expression showed dramatic reduction in NF-κB activation and IL-6 production and were less sensitive to Bay 11-7082 in clonogenic survival assays (Supplementary Fig. S2C-F). Finally, C9b expression in HBEC-3KT/KP cells drove subcutaneous tumor growth in SCID mice (Fig. 1I), the hallmark of full cellular transformation. Specifically, thirty percent of mice (n=6/20) implanted with HBEC-3KT/KP cells expressing C9b developed tumors by 30 days post injection compared to none for those with GFP or 10% for AT/GG Mut C9b (n=1/10 of a significantly smaller size than WT C9b) (Fig. 1I and Supplementary Fig. S3). These tumors showed expression of Myc-tagged C9b (Fig.1I). Thus, C9b activates the NF-κB pathway and cooperates with oncogenic *KRAS* and p53 downregulation to drive full cellular transformation.

Expression of caspase 9b in mouse pneumocytes activates the NF-κB pathway in vivo.

As C9b enhanced tumorigenic phenotypes and cellular transformation, we next examined whether these biological phenotypes translated *in vivo*. To study the role of C9b in lung pathophysiology and tumorigenesis *in vivo*, we generated transgenic mouse lines expressing human C9b under the surfactant protein C (SPC) promoter that confers lung epithelium-specific expression in alveolar type II pneumocytes and bronchioalveolar cells (25,26) (Fig. 2A). Among the independent founder lines, line 2 and line 4 mice showed germline transmission and both high C9b mRNA and protein expression restricted to the lung (Fig. 2B-D). These mice were also viable and fertile with no gross differences compared to transgene negative control mice.

Since C9b directly activated NF-κB pathway in primary lung epithelial and NSCLC cell lines (6), we tested the effects of C9b expression in mouse lung for induction of this pathway. First, C9b expression in lung epithelial cells was confirmed by immunohistochemical staining with FLAG and C9 antibodies (Fig. 2E). Importantly, lungs of these mice showed decreased levels of IκBα, increased levels of phospho-p65, and enhanced nuclei localizations of p65 compared to those of littermate transgene negative control mice (Fig. 2E). Thus, C9b mice demonstrated NF-κB pathway activation in mouse lungs showing the translation of previous *in vitro* findings to the *in vivo* setting.

Expression of human caspase 9b in mice pneumocytes induces lung inflammation and immune cell infiltration.

Previously NF-κB activation induced in all lung epithelium was shown to cause an emphysema phenotype and infiltration of immune cells (15), and thus, we next histologically evaluated the effect of C9b expression on lung inflammation. Compared to control mice, C9b mice, even though C9b is only expressed in a subset of lung epithelial cells, demonstrated an emphysema phenotype in the presentation of enlarged alveolar ducts and alveolar sacs (Fig. 2E &3 A, B). The average size of the alveolar sac was significantly larger

in C9b mice (6-8 months old) for both line 2 (2093 ± 360.8, n=5, p=0.0283) and line 4 (2223 ± 441.3, n=5, p=0.0193) compared to control mice (832.8 ± 82.26, n=5) (Fig. 3A,B). Fibrosis and fibrotic thickening of small airway walls and alveoli was evident with increased collagen deposition in C9b mice by trichrome staining (Fig. 3A). In addition, increased perivascular and peribronchiolar lymphoid aggregates and diffuse inflammation were observed in the lungs of C9b mice (Fig. 3C,D). Both Line 2 (average lung inflammation score 1.5 ± 0.189, n=7, p=0.0026) and line 4 (1.78 ± 0.278, n=9, p=0.0010) C9b mice showed increased numbers and sizes of immune aggregates and diffuse inflammation in lung parenchyma compared to littermate controls (0.57 ± 0.165, n=14, Fig. 3C,D). Analysis of the immune cell populations increased in the lungs of C9b mice included Gr1+ neutrophils, monocytes, macrophages, and myeloid derived suppressor cells (MDSCs) as well as CD3ε+ T cells, B220+ B cells, CD44+ memory T cells, OX40+ effector T cells, Mac-2+ histiocytes (Supplementary Fig. S4A). Flow cytometry analysis of cells prepared from whole lungs and spleens showed increased effector/effector memory CD4+ and CD8+ T cell populations in lung and spleen of C9b mice compared to control mice as defined by CD44+ and CD62L+ (Supplementary Fig. S4B). The most significant changes were the increased percentage of MDSCs (Gr1+ and CD11b+) in the lungs and spleens of C9b mice compared to control (Fig. 3E,F). Thus, C9b mice demonstrated significant lung inflammation indicative of constitutive activation of the NF-κB pathway through a presentation of remodeling of lung epithelium with emphysema, fibrosis, increased lymphoid aggregates, and increased infiltration of MDSCs.

Expression of human caspase 9b in mice pneumocytes is linked to skin dermatitis.

One unexpected phenotype observed among C9b mice was the development of severe skin dermatitis (Fig. 4A) as the C9b transgene was not expressed in the keratinocytes, fibroblasts, and melanocytes in the skin of C9b mice (Supplementary Fig. S4C). Specifically, a cohort of Line 2 (n=74) and line 4 (n=36) C9b mice were compared to littermate control mice (n=68) from 3 months to 23 months of age. Although skin dermatitis is common around the neck and body of female C57BL/6 strain mice (19), C9b mice developed severe ulcerative lesions often on the face with deep scabs warranting euthanasia, affecting both male and female mice (Fig. 4; Supplementary Fig. S5). Kaplan-Meier dermatitis-free survival curves show significantly increased severe dermatitis development both in line 2 ($p<0.001$, Log-rank test) and line 4 (p=0.0029) compared to control mice (Fig. 4B). Histological analysis of the skin lesions showed the epidermal hyperplasia, serocellular crusting, and dermal inflammatory infiltrates (Fig. 4C) as well as thickened and disorganized dermal collagen layers (Fig. 4C). Thus, C9b mice with C9b expression in lung pneumocytes showed systemic inflammatory phenotypes.

To begin to determine the mechanistic underpinnings of how C9b mice develop skin inflammatory phenotypes distal from lungs where it is expressed, the levels of cytokines/chemokines in blood circulation were assessed. Various cytokines/chemokines such as CXCL13, IL-16, IL-1Rα, CCL5, CCL2, G-CSF, CXCL1, and TIMP1 were all up-regulated in the plasma of C9b mice with dermatitis compared to control (Supplementary Fig. S6A). Previously, we identified *CXCL1* and *CXCL2,* downstream targets of NF-κB pathway that were associated with atopic dermatitis (46), as genes regulated by C9b (6). Here,

we observed increased expression of *Cxcl1* and/or *Cxcl2* in lungs of C9b mice that were suppressed by IκBα super repressor (Supplementary Fig. S6B-D). The NF-κB pathway is also known to activate the proinflammatory cytokine IL-6, which is a known regulator of the survival and expansion of MDSCs as well as skin dermatitis and wound healing (27,28). We found that reduced C9b expression and Bay 11-7082 treatment in A549 cells suppressed IL-6 secretion and IL-6 mRNA expression as well as CXCL1 expression (Supplementary Fig. S2). IL-6 levels in the blood of control vs. C9b mice were significantly increased (both line 2 (204.8 ± 51.40, n=23, p=0.0018) and line 4 (82.65 ± 17.11, n=11, p=0.0057) as well as significantly increased plasma IL-6 levels (Supplementary Fig. S6E) compared to control groups (20.72 ± 8.78 pg/ml. When mice were grouped based on the presence and absence of skin dermatitis, IL-6 levels were increased compared to control in line 2 (298.2 ± 97.12, n=10, p=0.0192) and line 4 (72.66 ± 9.816, n=8, p=0.0012) C9b mice without dermatitis (Supplementary Fig. S6F). These results show that the increase of plasma IL-6 is not caused by dermatitis, but by C9b expression in the lung driving not only a localized, but also a more systemic inflammatory response. Since these are only correlative observations, identification of causal cytokines/chemokines driving skin phenotypes of the C9b mice require further studies.

C9b mice develop lung cancer with aging.

To investigate whether C9b expression in lung epithelium promotes lung tumorigenesis, aged C9b mice (>21 months old) were compared to age-matched control mice. Consistent to the low spontaneous lung cancer incidents (1% in males, 3% in breeding females, and 0% in virgin females) in C57BL/6J mice (strain background of C9b mice), none of the control (n=0/20) mice developed primary lung cancers (29). In stark contrast, various histological subtypes of lung cancers were observed in C9b mice (n=4/20 for line 2 and n=2/13 for line 4, Fig, 5A.B) in addition to emphysema, fibrosis, and severe inflammation associated with the increased infiltration of macrophages and lymphocytes (Supplementary Fig. S7A). Histological subtypes include squamous cell carcinoma (n=1, p63 positive) and carcinoid tumor (n=1, synaptophysin positive), and adenocarcinomas. Adenocarcinoma was the most common subtype observed (n=3/20 for line 2 and n=2/13 for line 4), which were negative for adenocarcinoma differentiation marker Nkx2.1, but positive for acidic/neutral mucin by Alcian blue-PAS staining (Fig. 5C). Unexpectedly, all these tumors were negative for SPC and FLAG-tagged C9b expression while surrounding normal epithelium were positive for SPC and FLAG (Fig. 5C). Most of these tumors were positive for SOX2 that were normally expressed in conducting, but not in respiratory airways. Thus, our data suggest that these tumors are derived from conducting airway cells or bronchioalveolar stem cells (BASCs) at the bronchioalveolar duct junction (BADJ) that can generate both conducting and respiratory airway cells including type II pneumocytes (SPC+)

To examine the modulating effect of C9b on the tumor microenvironment, the number of MDSCs in the C9b mice lung tumors were examined as MDSCs (Gr1+/CD11b+) have been shown to promote tumor growth (30). C9b mice both with (Gr1+ cells per 20x field, 47.5 ± 11.7) or without lung tumors (57.1 ± 20.5) show significantly increased Gr1+ cells infiltrating into lung parenchyma compared to control (7.26 ± 4.14) (Fig. 5D,E), suggesting that elevation of MDSCs is not consequence of the tumor formation, but is more likely

due to C9b expression. In addition, type II pneumocytes, not tumor cells, express IL-6 (Supplementary Fig. S7B). These data show that C9b enhances the recruitment of MDSCs into the lung allowing for a pro-tumor microenvironment.

C9b cooperates with KRAS in lung tumorigenesis.

Based on our finding that C9b will cooperate with oncogenic *KRAS* to induce cellular transformation and provides a pro-tumorigenic microenvironment, we hypothesized that C9b expression will cooperate with oncogenic *KRAS* to drive lung tumorigenesis. To test this hypothesis, $KRAS^{G12D}$ L/+ mice were intratracheally injected with modular lentiviral particles (31) to simultaneously express Cre recombinase and a coding sequence (CDS) of either GFP (n=12), WT C9b (n=10), or AT/GG Mut C9b (n=11) (Fig. 6A, B). At 32 wks post injection, lungs from GFP control mice showed tumor foci with ERK activation, a sign of *KRAS* activation (Fig 6C). WT C9b expression led to the development of larger sized and increased tumor multiplicity compared to GFP controls as assayed by percent replacement of normal lung parenchyma by tumor cells based on H&E and pERK signal (Fig. 6C, D; GFP 4%, WT C9b 37%). Mut C9b also significantly enhanced these parameters, but to a lesser extent than WT C9b (Mut C9b 21%). Interestingly, tumors driven by WT C9b showed dramatically stronger HMGA2 expression in a high percentage of tumor cells compared to tumors from control GFP or Mut C9b expression (Fig. 6E), which is a hallmark of a shift to poorly differentiated and more invasive tumors. We also observed a case of distal metastatic lung tumor with desmoplastic reaction (Fig. 6F) with only WT C9b. In addition, numerous clusters of immune cell foci were observed in or near tumors in WT C9b group. C9b expression in the context of *KRAS* activation *in vivo* also increased the number of Gr1+ cells infiltrated into lungs compared to GFP (36.8±21.2 vs. 4.9±4.6, p=0.0022) and to Mut C9b (8.3±4.0, p<0.0001) (Fig. 6G; Supplementary Fig. S7). Mut C9b did not increase Gr1+ cells in lung compared to GFP (p=0.5607) (Fig. 6G). To assess whether this increase in Gr1+ cells correlates with increased MDSCs, we analyzed % of Gr1+ CD11b+ cells in the lungs by FACS analyses (n=2 each, Supplementary Fig. S8). Lungs with WT C9b showed a higher percentage of MDSCs compared to GFP or Mut C9b. Thus, WT C9b cooperated with *KRAS* activation, driving more poorly differentiated lung tumors with an increase in infiltrating MDSCs (or Gr1+ high immune infiltrates), while Mut C9b also moderately enhanced lung tumorigenesis, but without increasing MDSCs. These data suggest a role for NF-κB activation by C9b via cIAP1 in recruiting or the expansion of MDSCs, which would provide a more pro-tumor microenvironment.

DISCUSSION

In this study, C9b expressed in the lung pneumocytes of mice activated the NF-κB pathway *in vivo*, induced lung inflammation, the infiltration of immune cells (e.g., immunosuppressive MDSCs conducive to tumor growth), affected the peripheral immune system, and induced systemic inflammation. Importantly, C9b induced lung tumor formation in aging mice and cooperated strongly with oncogenic *KRAS* to enhance both cellular transformation and lung tumorigenesis. HMGA2 expression was dramatically increased in tumors from the oncogenic KRAS mice by WT C9b. HMGA2 is upregulated in lung cancer, a hallmark of higher grade tumors, highly expressed in poorly differentiated and

invasive cancers, and inversely correlated with survival (32,33). Thus, C9b is driving the formation of high grade lung tumors, which required the ability of C9b to associate with cIAP1 as expression of a well-characterized, structurally intact mutant of C9b lacking the ability to bind cIAP1 showed significantly less ability to enhance lung tumorigenesis in cooperation with *KRAS*. Therefore, the presented study corroborates the previous findings of both the Jacks and Baldwin laboratories in the cooperation of the NF-κB pathways in oncogenic *KRAS*-induced lung tumorigenesis and induction of higher grade tumors (11,12), but importantly, provides a physiologic and mechanistic link to the alternative splicing of *CAS9* to produce C9b and activate this system. This finding translated to the ability of C9b to induce cellular transformation in cooperation with oncogenic *KRAS* and oncogenic *KRAS/TP53* downregulation. Thus, the C9b/cIAP1 interaction site may be a plausible personalized therapeutic target for NSCLC expressing higher levels of C9b without the global effects on suppressing the immune system such as the concerns for general NF-κB inhibitors.

As we observed the spontaneous induction of lung tumors in the C9b mice in stark contrast to WT mice, C9b may be, by definition, a protooncogene, explaining the enhanced C9b expression observed in a large percentage of NSCLC tumors. On the other hand, many of the spontaneous tumors from the aging C9b transgenic mice showed expression of SOX2, and all lacked expression of SPC and our C9b transgene (expressed via an SPC promotor). SOX2 is a transcription factor playing essential roles in lung development and maturation. SOX2 is expressed in the trachea, airway/bronchiolar epithelium and the conducting airways of the adult lung, but is completely absent from the respiratory airways (34). Previously, SOX2 was proposed to differentiate $KRAS^{G12C}$ driven tumors as derived from Clara cell antigen 10 (CC10) + cells, not from SPC+ cells (35,36). Our data suggest that these tumors are either derived from transformed (CC10)-expressing cells or bronchioalveolar stem cells (BASCs) at the bronchioalveolar duct junction (BADJ) coexpressing CC10 and SPC. SPC (and thus, C9b under an SPC promotor) is downregulated as tumors progress (37). This possibly explains the loss of C9b expression in the spontaneous lung tumors observed in the C9b mice if C9b is a protooncogene. Conversely, C9b expression alone does not confer *in vitro* cellular transformation to the HBEC-3KT cells, and thus, the role of C9b may be as an extrinsic paracrine role in modulating the microenvironment allowing tumor growth to occur in a more spontaneous manner. Additional studies are needed to determine whether C9b is truly a protooncogene or acts to promote a strong pro-tumorigenic microenvironment.

Mechanistically, C9b plays NF-κB-dependent and -independent functions as we have previously reported (6). NF-κB activates myriads of downstream target genes such as c-Myc and C/EBPα and various cytokine/chemokines (38,39). Thus, C9b is expected to alter many of these genes leading to the inflammatory phenotypes observed. In fact, we observed that reduced C9b expression (via siRNA targeting C9b) downregulated C/EBPα (Supplementary Figure S9A). Bay 11-7082, NF-κB pathway inhibitor, suppressed C/EBPα level in A549 (Supplementary Figure S9B). These data suggest that C/EBPα may be downstream of C9b activation of the NF-κB pathway (as one of the many transcription factors regulated by NF-κB such as c-Myc). In addition, the NF-κB-independent, anti-apoptotic function of C9b did significantly enhance tumor area/multiplicity induced by oncogenic *KRAS* as shown by expression of the Mut C9b, which retains the ability to bind APAF1, block activation

of C9a, and inhibit intrinsic apoptosis. Our findings suggest that loss of intrinsic apoptosis in cells such as would be observed by loss of the *CAS9* gene would support cooperation with oncogenes to drive cell transformation and lung tumor formation. Currently, the role of the *CAS9* gene as a tumor suppressor is controversial with Lowe and co-workers reporting the loss of the CAS9 enhances the cellular transformation of murine embryonic fibroblasts induced by oncogenic manipulations (3); a finding that was not confirmed by Strasser and co-workers (40). Our findings suggest that in certain contexts, C9a will act as a tumor suppressor, at least in constraining the ability of tumors to transition to higher grades. This study also found that expression of the Mut C9b significantly enhanced *in vitro* cell transformation in cooperation with oncogenic *KRAS*, albeit to a much lesser extent than WT C9b that retains the ability to also drive the NF-κB pathway. On the other hand, Mut C9b only induced full cellular transformation in cooperation with oncogenic manipulations in one instance, and thus, a full tumor suppressive role for the anti-apoptotic functions of the *CAS9* gene requires more exploration in different cellular and oncogenic contexts.

Another novel finding was the systemic nature of inflammation that was observed by early activation of the NF-κB pathway in only lung pneumocytes induced by C9b expression. Indeed, systemic inflammation was observed as shown by increased serum levels of various cytokines (Ex. CXCL1 and IL-6) and facial dermatitis. NF-κB family of transcription factors have been implicated in the pathogenesis of several autoimmune diseases including rheumatoid arthritis, inflammatory bowel disease, type I diabetes, systemic lupus erythematosus and multiple sclerosis (41). Interestingly, mouse models with altered NF-κB pathway have shown skin dermatitis phenotypes. For example, IκBα −/− mice was reported to develop widespread severe skin dermatitis with increased Cd11b+ macrophages/monocytes in spleen (42) and *cRel−/−p50−/−p65+/−* mice developed spontaneous dermal and intestinal inflammation in association with chronic neutrophilia (39). Clinical links are also reported between facial rashes and lung inflammation as to asthma and viral pneumonia induced by COVID-19 (43-45). Whereas the clinical manifestation of the facial rash was suggested as a plausible link to the later development of asthma, our findings suggest the opposite in that lung inflammation, not yet manifested or detectable by current clinical tests, is prognostic for later development of asthma. In these cases, clinical testing for systemic IL-6 may be suggested to treat the lung inflammation to block the development of chronic lung disease. Of note, this study is mainly showing correlative observations between C9b, NF-κB activation in the Type II pneumocytes, and systemic inflammation linked to facial dermatitis. The identification of causal cytokines/chemokines driving skin phenotypes of the C9b mice require further studies, but our findings suggest a very strong interplay between organ systems and systemic inflammation.

In conclusion, this study found that C9b induces the activation of the NF-κB pathway in the lungs, the infiltration of lymphocytes into the lungs, and lung inflammation linked to increased IL-6 levels, systemic inflammation, and facial dermatitis. C9b induced lung tumor formation in aged mice demonstrating that C9b is either a protooncogene, promotes a highly pro-tumor microenvironment, or both, leading to spontaneous tumor formation. C9b also cooperated with oncogenic *KRAS* to induce lung tumorigenesis, which identified the C9b/cIAP1 interaction as a plausible new target for personalized treatment of NSCLC presenting with high C9b expression.

Supplementary Material

Refer to Web version on PubMed Central for supplementary material.

ACKNOWLEDGEMENTS

This work was supported by the National Institutes of Health (NIH) –National Institute of General Medical Sciences grant, R01 GM137578 (to CEC). This work was also supported by research grants from the Veteran's Administration (VA Merit Review I, BX001792 (CEC) and a Senior Research Career Scientist Award, IK6BX004603 (CEC)). S. Kim was supported in part by NIH/National Cancer Institute MERIT Award (5R37CA248298 to SK) and M. Kim was supported by Bankhead-Coley Cancer Research Bridge Award (9BC15 to MK). The contents of this manuscript do not represent the views of the Department of Veterans Affairs or the United States Government.

REFERENCES

1. Li P, Zhou L, Zhao T, Liu X, Zhang P, Liu Y, et al. Caspase-9: structure, mechanisms and clinical application. Oncotarget 2017;8:23996–4008 [PubMed: 28177918]
2. Shultz JC, Chalfant CE. Caspase 9b: a new target for therapy in non-small-cell lung cancer. Expert Rev Anticancer Ther 2011;11:499–502 [PubMed: 21504315]
3. Soengas MS, Alarcon RM, Yoshida H, Giaccia AJ, Hakem R, Mak TW, et al. Apaf-1 and caspase-9 in p53-dependent apoptosis and tumor inhibition. Science 1999;284:156–9 [PubMed: 10102818]
4. Srinivasula SM, Ahmad M, Guo Y, Zhan Y, Lazebnik Y, Fernandes-Alnemri T, et al. Identification of an endogenous dominant-negative short isoform of caspase-9 that can regulate apoptosis. Cancer Res 1999;59:999–1002 [PubMed: 10070954]
5. Seol DW, Billiar TR. A caspase-9 variant missing the catalytic site is an endogenous inhibitor of apoptosis. J Biol Chem 1999;274:2072–6 [PubMed: 9890966]
6. Vu NT, Park MA, Shultz MD, Bulut GB, Ladd AC, Chalfant CE. Caspase-9b Interacts Directly with cIAP1 to Drive Agonist-Independent Activation of NF-kappaB and Lung Tumorigenesis. Cancer Res 2016;76:2977–89 [PubMed: 27197231]
7. Goehe RW, Shultz JC, Murudkar C, Usanovic S, Lamour NF, Massey DH, et al. hnRNP L regulates the tumorigenic capacity of lung cancer xenografts in mice via caspase-9 pre-mRNA processing. J Clin Invest 2010;120:3923–39 [PubMed: 20972334]
8. Shultz JC, Goehe RW, Wijesinghe DS, Murudkar C, Hawkins AJ, Shay JW, et al. Alternative splicing of caspase 9 is modulated by the phosphoinositide 3-kinase/Akt pathway via phosphorylation of SRp30a. Cancer Res 2010;70:9185–96 [PubMed: 21045158]
9. Balkwill F, Mantovani A. Inflammation and cancer: back to Virchow? Lancet 2001;357:539–45 [PubMed: 11229684]
10. Xia Y, Shen S, Verma IM. NF-kappaB, an active player in human cancers. Cancer Immunol Res 2014;2:823–30 [PubMed: 25187272]
11. Basseres DS, Ebbs A, Levantini E, Baldwin AS. Requirement of the NF-kappaB subunit p65/RelA for K-Ras-induced lung tumorigenesis. Cancer Res 2010;70:3537–46 [PubMed: 20406971]
12. Meylan E, Dooley AL, Feldser DM, Shen L, Turk E, Ouyang C, et al. Requirement for NF-kappaB signalling in a mouse model of lung adenocarcinoma. Nature 2009;462:104–7 [PubMed: 19847165]
13. Han W, Joo M, Everhart MB, Christman JW, Yull FE, Blackwell TS. Myeloid cells control termination of lung inflammation through the NF-kappaB pathway. Am J Physiol Lung Cell Mol Physiol 2009;296:L320–7 [PubMed: 19098124]
14. Sheller JR, Polosukhin VV, Mitchell D, Cheng DS, Peebles RS, Blackwell TS. Nuclear factor kappa B induction in airway epithelium increases lung inflammation in allergen-challenged mice. Exp Lung Res 2009;35:883–95 [PubMed: 19995280]
15. Zaynagetdinov R, Sherrill TP, Gleaves LA, Hunt P, Han W, McLoed AG, et al. Chronic NF-kappaB activation links COPD and lung cancer through generation of an immunosuppressive microenvironment in the lungs. Oncotarget 2016;7:5470–82 [PubMed: 26756215]

16. Sato M, Vaughan MB, Girard L, Peyton M, Lee W, Shames DS, et al. Multiple oncogenic changes (K-RAS(V12), p53 knockdown, mutant EGFRs, p16 bypass, telomerase) are not sufficient to confer a full malignant phenotype on human bronchial epithelial cells. Cancer Res 2006;66:2116–28 [PubMed: 16489012]
17. Wikenheiser KA, Vorbroker DK, Rice WR, Clark JC, Bachurski CJ, Oie HK, et al. Production of immortalized distal respiratory epithelial cell lines from surfactant protein C/simian virus 40 large tumor antigen transgenic mice. Proc Natl Acad Sci U S A 1993;90:11029–33 [PubMed: 8248207]
18. Serre J, Tanjeko AT, Mathyssen C, Vanherwegen AS, Heigl T, Janssen R, et al. Enhanced lung inflammatory response in whole-body compared to nose-only cigarette smoke-exposed mice. Respir Res 2021;22:86 [PubMed: 33731130]
19. Williams-Fritze MJ, Carlson Scholz JA, Zeiss C, Deng Y, Wilson SR, Franklin R, et al. Maropitant citrate for treatment of ulcerative dermatitis in mice with a C57BL/6 background. J Am Assoc Lab Anim Sci 2011;50:221–6 [PubMed: 21439216]
20. Jackson EL, Willis N, Mercer K, Bronson RT, Crowley D, Montoya R, et al. Analysis of lung tumor initiation and progression using conditional expression of oncogenic K-ras. Genes Dev 2001;15:3243–8 [PubMed: 11751630]
21. Hill KS, Roberts ER, Wang X, Marin E, Park TD, Son S, et al. PTPN11 Plays Oncogenic Roles and Is a Therapeutic Target for BRAF Wild-Type Melanomas. Mol Cancer Res 2019;17:583–93 [PubMed: 30355677]
22. MacKnight HP, Stephenson DJ, Hoeferlin LA, Benusa SD, DeLigio JT, Maus KD, et al. The interaction of ceramide 1-phosphate with group IVA cytosolic phospholipase A2 coordinates acute wound healing and repair. Sci Signal 2019;12
23. Hamaidi I, Zhang L, Kim N, Wang MH, Iclozan C, Fang B, et al. Sirt2 Inhibition Enhances Metabolic Fitness and Effector Functions of Tumor-Reactive T Cells. Cell Metab 2020;32:420–36 e12 [PubMed: 32768387]
24. Sato M, Larsen JE, Lee W, Sun H, Shames DS, Dalvi MP, et al. Human lung epithelial cells progressed to malignancy through specific oncogenic manipulations. Mol Cancer Res 2013;11:638–50 [PubMed: 23449933]
25. Wert SE, Glasser SW, Korfhagen TR, Whitsett JA. Transcriptional elements from the human SP-C gene direct expression in the primordial respiratory epithelium of transgenic mice. Dev Biol 1993;156:426–43 [PubMed: 8462742]
26. Glasser SW, Burhans MS, Eszterhas SK, Bruno MD, Korfhagen TR. Human SP-C gene sequences that confer lung epithelium-specific expression in transgenic mice. Am J Physiol Lung Cell Mol Physiol 2000;278:L933–45 [PubMed: 10781423]
27. Johnson BZ, Stevenson AW, Prele CM, Fear MW, Wood FM. The Role of IL-6 in Skin Fibrosis and Cutaneous Wound Healing. Biomedicines 2020;8
28. Condamine T, Gabrilovich DI. Molecular mechanisms regulating myeloid-derived suppressor cell differentiation and function. Trends Immunol 2011;32:19–25 [PubMed: 21067974]
29. Hoag WG. Spontaneous cancer in mice. Ann N Y Acad Sci 1963;108:805–31 [PubMed: 14081516]
30. Gabrilovich DI. Myeloid-Derived Suppressor Cells. Cancer Immunol Res 2017;5:3–8 [PubMed: 28052991]
31. Geiling B, Vandal G, Posner AR, de Bruyns A, Dutchak KL, Garnett S, et al. A modular lentiviral and retroviral construction system to rapidly generate vectors for gene expression and gene knockdown in vitro and in vivo. PLoS One 2013;8:e76279 [PubMed: 24146852]
32. Sarhadi VK, Wikman H, Salmenkivi K, Kuosma E, Sioris T, Salo J, et al. Increased expression of high mobility group A proteins in lung cancer. J Pathol 2006;209:206–12 [PubMed: 16521118]
33. Huang B, Yang J, Cheng Q, Xu P, Wang J, Zhang Z, et al. Prognostic Value of HMGA2 in Human Cancers: A Meta-Analysis Based on Literatures and TCGA Datasets. Front Physiol 2018;9:776 [PubMed: 29997523]
34. Kapere Ochieng J, Schilders K, Kool H, Buscop-van Kempen M, Boerema-De Munck A, Grosveld F, et al. Differentiated type II pneumocytes can be reprogrammed by ectopic Sox2 expression. PLoS One 2014;9:e107248 [PubMed: 25210856]

35. Xu X, Rock JR, Lu Y, Futtner C, Schwab B, Guinney J, et al. Evidence for type II cells as cells of origin of K-Ras-induced distal lung adenocarcinoma. Proc Natl Acad Sci U S A 2012;109:4910–5 [PubMed: 22411819]

36. Sutherland KD, Song JY, Kwon MC, Proost N, Zevenhoven J, Berns A. Multiple cells-of-origin of mutant K-Ras-induced mouse lung adenocarcinoma. Proc Natl Acad Sci U S A 2014;111:4952–7 [PubMed: 24586047]

37. Li B, Meng YQ, Li Z, Yin C, Lin JP, Zhu DJ, et al. MiR-629-3p-induced downregulation of SFTPC promotes cell proliferation and predicts poor survival in lung adenocarcinoma. Artif Cells Nanomed Biotechnol 2019;47:3286–96 [PubMed: 31379200]

38. Wang D, Paz-Priel I, Friedman AD. NF-kappa B p50 regulates C/EBP alpha expression and inflammatory cytokine-induced neutrophil production. J Immunol 2009;182:5757–62 [PubMed: 19380823]

39. von Vietinghoff S, Asagiri M, Azar D, Hoffmann A, Ley K. Defective regulation of CXCR2 facilitates neutrophil release from bone marrow causing spontaneous inflammation in severely NF-kappa B-deficient mice. J Immunol 2010;185:670–8 [PubMed: 20519647]

40. Scott CL, Schuler M, Marsden VS, Egle A, Pellegrini M, Nesic D, et al. Apaf-1 and caspase-9 do not act as tumor suppressors in myc-induced lymphomagenesis or mouse embryo fibroblast transformation. J Cell Biol 2004;164:89–96 [PubMed: 14709542]

41. Sun SC, Chang JH, Jin J. Regulation of nuclear factor-kappaB in autoimmunity. Trends Immunol 2013;34:282–9 [PubMed: 23434408]

42. Klement JF, Rice NR, Car BD, Abbondanzo SJ, Powers GD, Bhatt PH, et al. IkappaBalpha deficiency results in a sustained NF-kappaB response and severe widespread dermatitis in mice. Mol Cell Biol 1996;16:2341–9 [PubMed: 8628301]

43. Genovese G, Moltrasio C, Berti E, Marzano AV. Skin Manifestations Associated with COVID-19: Current Knowledge and Future Perspectives. Dermatology 2021;237:1–12 [PubMed: 33232965]

44. Luo J, Li Y, Gong R. The mechanism of atopic march may be the 'social' event of cells and molecules (Review). Int J Mol Med 2010;26:779–85 [PubMed: 21042770]

45. Peters N, Peters AT. Atopic dermatitis. Allergy Asthma Proc 2019;40:433–6 [PubMed: 31690388]

46. Deftu AF, Filippi A, Shibsaki K, Gheorghe RO, Chiritoiu M, Ristoiu V. Chemokine (C-X-C motif) ligand 1 (CXCL1) and chemokine (C-X-C motif) ligand 2 (CXCL2) modulate the activity of TRPV1+/IB4+ cultured rat dorsal root ganglia neurons upon short-term and acute application. J Physiol Pharmacol. 2017 Jun;68(3):385–395. [PubMed: 28820395]

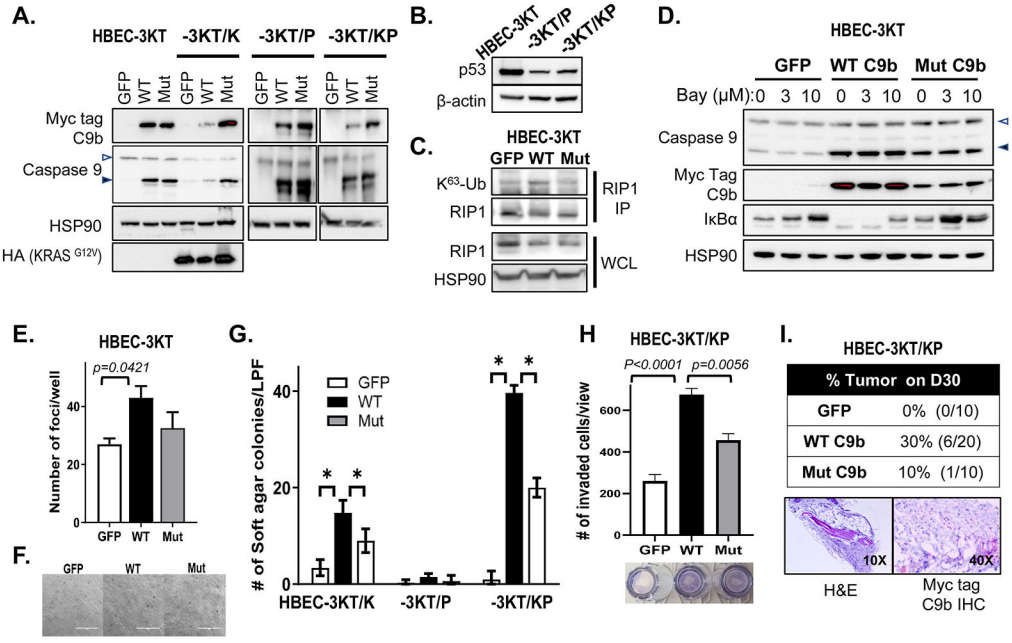

Figure 1. C9b activates NF-κB in HBEC-3KT cells and cooperates with *KRAS* activation and p53 loss driving anchorage independent growth (AIG) and invasion *in vitro* and tumor growth *in vivo*.

A-D. Western blot analyses with indicated antibodies of HBEC-3KT, −3KT/K (*KRAS*^{G12V}), −3KT/P (sh*TP53*), and −3KT/KP cells expressing GFP, wild type (WT), or AT/GG mutant (Mut) C9b (with a Myc-tag). **C.** RIP1 immunoprecipitation (IP) followed by immunoblotting with K^{63}-Ub antibody shows increased RIP1 K^{63}-Ub by WT C9b in HBEC-3KT cells (in growth supplement free media). In **D**, HBEC-3KT cells were treated with 0, 3, 10 μM Bay 11-7082 for 15 h. WCL: whole cell lysates. The empty and filled triangles denote C9a and C9b proteins, respectively. **E.** Clonogenic assays of parental HBEC-3KT cells expressing GFP, WT, or Mut C9b. The graph shows numbers of clonal foci per well on D10. **F.** Bright field images (10x) of HBEC-3KT cells expressing GFP, WT, or Mut C9b grown in soft agar on D45. **G.** Number of colonies per low power filed (LPF) view grown in soft agar on D45 (*: p≤0.0002). **H.** Number of invaded HBEC-3KT/KP cells expressing GFP, WT, or Mut C9b through Matrigel at 22 h per LPF view. **I.** SCID Tumor take rate of HBEC-3KT/KP cells expressing GFP, WT, or Mut C9b on day 30 post implantation (top) and H&E, Myc-tag, and c-Myc IHC images (bottom panels). Data are means ± SD; n = 3 each. Adjusted *p* values are determined by ANOVA Tukey's multiple comparison test.

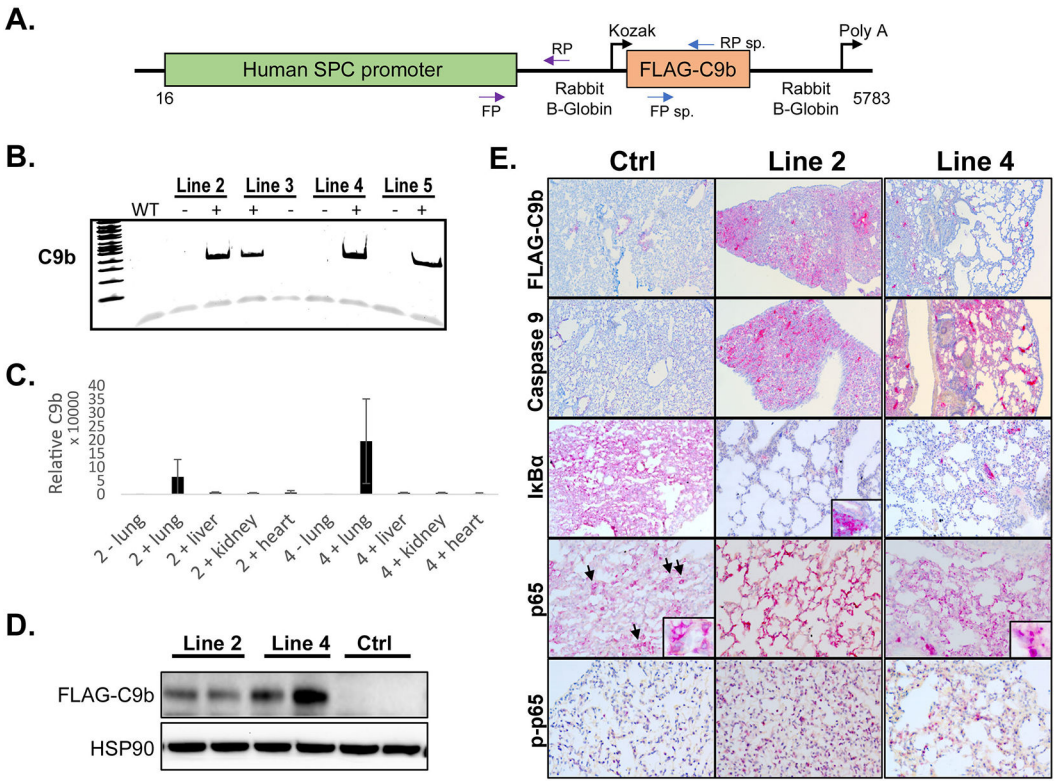

Figure 2. The SPC-driven C9b expression in mouse lung epithelium activates NF-κB pathway.

A. A schematic diagram of a C9b transgene construct driven by human SPC promoter. Among the C9b transgene positive founder lines (**B**, PCR), line 2 and 4 C9b+ mice showed high levels of C9b transgene expression in lungs both for mRNA (**C**, real time rt-PCR, relative ratio of C9b/GAPDH) and protein (**D**, western blot). **E.** Representative images of immunohistochemical staining with indicated antibodies (10x). Note a Flag-tagged C9b expression in lung epithelium, a decreased level of IκBα and an increased level of p-p65 in line 2 and line 4 mice compared to control mice. Insets (40x) in p65 images show the exclusion of p65 from nuclei in control but not in C9b mice. Inset in IκBa shows its strong positivity in immune aggregates.

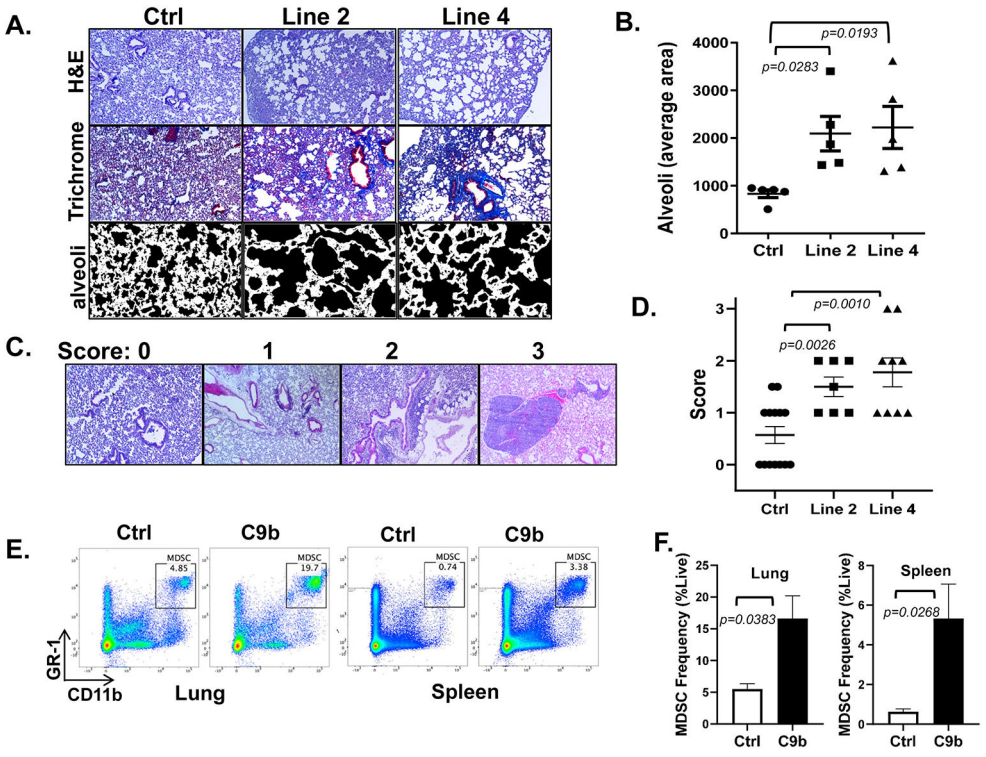

Figure. 3. Lungs of C9b mice show emphysema, fibrosis, and immune infiltration.

A. H&E and trichrome staining show enlarged alveoli and increased peribronchovascular collagen deposits in line 2 and line 4 mice compared to control. Average area of alveoli (**B**, n=5 per group) is measured using Image J from trichrome stained slides avoiding large vessels and bronchi (**A**, bottom row). **C,D**. Scoring systems for immune aggregates and infiltrates (**C,** 10X) and average lung inflammation score for each group (n=14 for control, 7 for line 2, and 9 for line 4 mice, **D)**. **E, F**. Increased % of MDSCs (Gr1+/CD11b+) in lung and spleen of C9b mice (n=3) compared to Control (n=3) by FACS analysis. Data are means ± SEM. Adjusted *p* values are determined by ANOVA Tukey's multiple comparison test for **B**&**D** and by unpaired t-test for **F**.

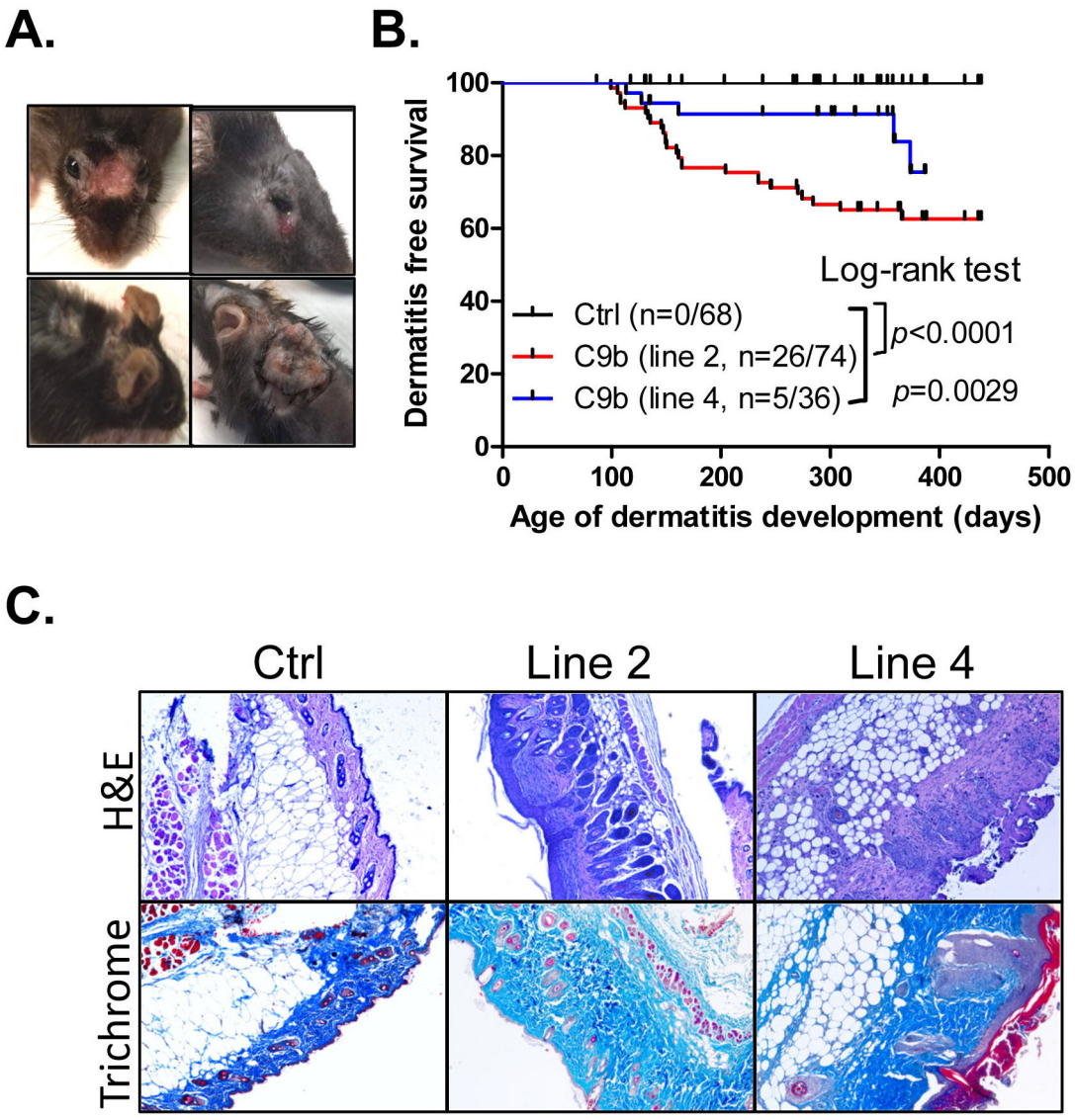

Figure 4. C9b mice develop severe skin dermatitis on the face and the back skin requiring euthanasia

(**A**). **B.** Kaplan-Meier dermatitis-free survival curves show early onset of dermatitis in line 2 (n=74) and line 4 mice (n=36) compared to control (n=68, *p* value: Log-rank test). **C.** H&E and trichrome staining of skins show the significantly thickened dermal area with increased collagen (blue in trichrome) in dermatitis lesions of C9b mice.

A

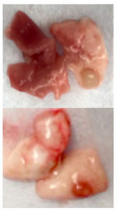

B

	% lung tumor	
Ctrl	0 % (0/20)	
Line 2	20% (4/20)	Adenocarcinoma (n=3), SCC (n=1), Carcinoid tumor* (n=1)
Line 4	15.4% (2/13)	Adenocarcinoma (n=2)

C

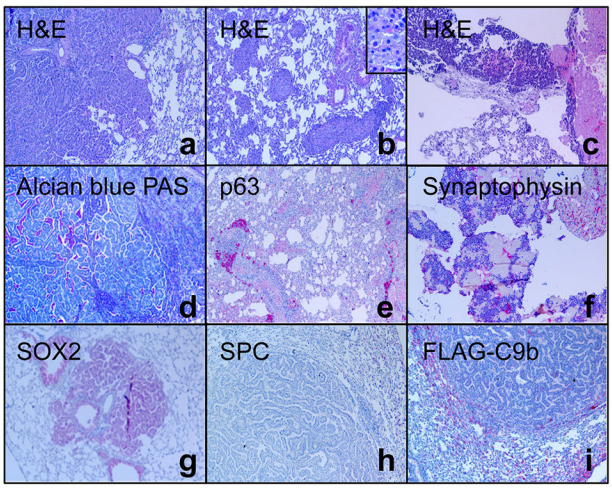

D

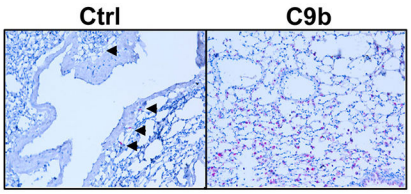

E

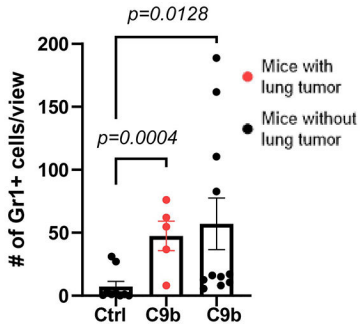

Figure 5. C9b mice develop lung tumors with aging.

Macroscopic (**A**) and microscopic lung tumors observed in C9b mice over 21m old of age are summarized in **B**. *: One mouse developed a carcinoid tumor and adenocarcinoma. **C.** Histological analyses including H&E (a-c), Alcian Blue-PAS (d), and IHC staining with indicated antibodies (e-i) of lung tumors identified adenocarcinoma (a,d, g-i), squamous cell carcinoma (scc, b&e), and carcinoid tumors (c&f). Images are taken at 10x magnification. Inset in b is at 40x magnification. **D&E.** Gr1+ cells (**D**, IHC) in the lung per low power field (20x, 3 views per mouse) were counted in control (n=9) and C9b mice with (red, n= 5) or without (n=11) lung tumors (**E**). Data are means ± SEM. Adjusted *p* values are determined by ANOVA with Tukey's multiple comparison test.

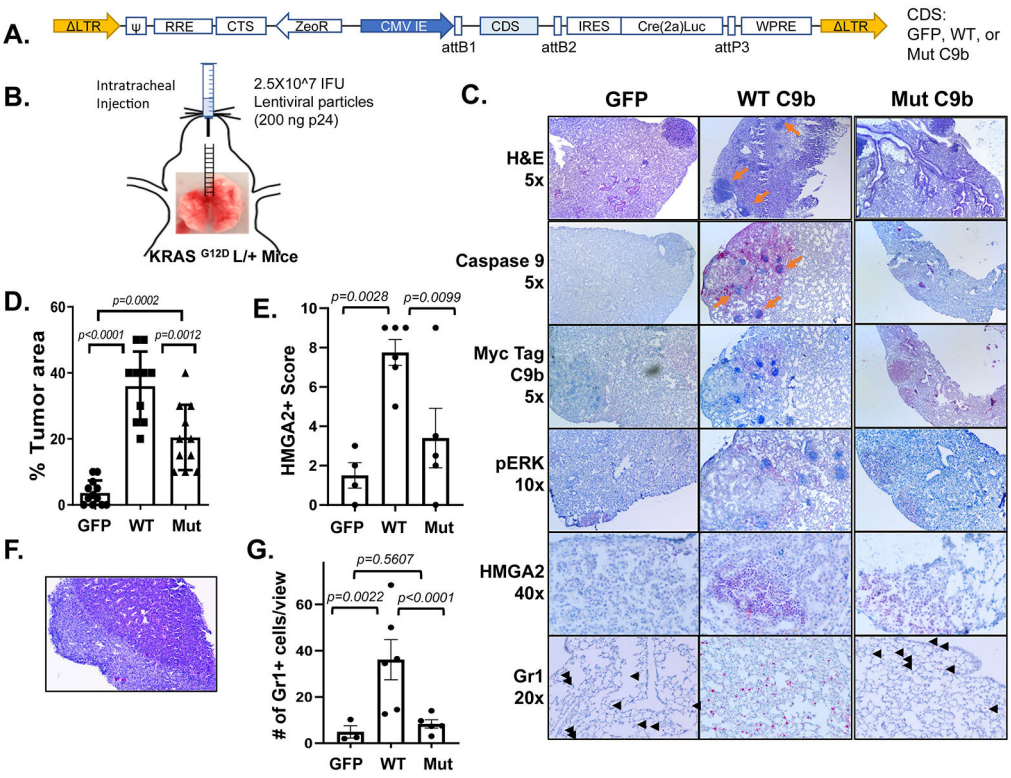

Figure 6. C9b cooperates with KRAS activation driving lung tumorigenesis.

KRAS^{G12D} L/+ mice with intratracheal injection (**B**) of lentiviral particles containing GFP-, WT-, or Mut C9b-Cre(T2a)Luc (**A**) developed lung tumors (**C**) at 32 wks post injection. Immunohistochemical staining (**C**) with indicated antibodies shows the expression of Myc-tagged WT or mutant C9b, ERK activation (pERK), and HMGA2 in tumors and the presence of Gr1+ cells in the lung (black arrowheads). Orange arrows point to the clusters of immune cells observed. The percent replacement of normal lung parenchyma by tumor cells based on H&E and pERK signal (n=12 for GFP, 10 for WT C9b, and 11 for Mut C9b, **D**), the HMGA2 positivity score (**E**), and the number of Gr1+ cells per view (20X magnification, **G**) (n=4 for GFP, 6 for WT C9b and Mut C9b, average of 3 views per mouse for **E**&**G**) in each group are shown. **F**. Metastasis observed in the liver (H&E, 10x magnification) in a mouse with WT C9b expression. Data in **D**,**E**,**G** are means ± SEM combined from 2 independent intratracheal injection experiments. Adjusted *p* values are determined by ANOVA Tukey's multiple comparison test.